



OPEN

Mechanism and significance of diffusion restriction followed by calcification in high-grade glioma treated with bevacizumab

Tomohiro Hosoya¹, Atsushi Kambe¹✉, Irfan Kesumayadi¹, Karen Makishima², Shuntaro Sueyoshi¹, Makoto Sakamoto¹ & Masamichi Kuroasaki¹

In this study, we focused on calcification and diffusion restriction, which sometimes appear around the resection cavity or periventricular white matter in patients with high-grade glioma (HGG) treated with bevacizumab (BVZ), as candidate imaging biomarkers for BVZ treatment efficacy. We investigated the timing of the appearance of diffusion restriction and calcification using magnetic resonance imaging and computed tomography in 35 patients with newly diagnosed or recurrent HGG treated with BVZ. In 17 (48.6%) patients, calcification was identified around the resection cavity or periventricular white matter at a median of 12 months after the initiation of BVZ treatment. Patients with calcification had significantly longer progression-free survival (16 vs. 7 months; $p = 0.0023$) and overall survival (36 vs. 12 months; $p = 0.0006$) than those without calcification. Histopathological examination revealed the presence of scattered microcalcifications within areas of necrosis, which suggested dystrophic calcification induced by BVZ. Diffusion-restricted lesions that appeared in patients with calcification had significantly lower apparent diffusion coefficients than those in patients without calcifications, indicating the presence of treatment-related necrosis but not hypercellularity. In conclusion, the radiological finding of diffusion restriction followed by calcification could be a potential imaging biomarker for favorable clinical course in patients with HGG treated with BVZ.

Keywords High-grade glioma, Bevacizumab, Calcification, Diffusion restriction, Survival

Vascular endothelial growth factor (VEGF) is a major inducer of tumor angiogenesis and promotes tumor growth by increasing vascular permeability and promoting cell migration¹. Anti-angiogenic agents exert antitumor effects by blocking the blood supply to tumors and causing hypoxia within tumor tissues. They are currently used to treat several solid tumors, including glioblastoma². Bevacizumab (BVZ), an anti-VEGF monoclonal antibody, was approved in 2009 by the United States Food and Drug Administration for use in patients with recurrent glioblastoma based on results showing decreased glucocorticoid use and longer progression-free survival (PFS)^{3,4}. The AVAglio trial, which verified the usefulness of BVZ for newly diagnosed glioblastoma, demonstrated prolonged PFS (10.6 months vs. 6.2 months) and longer maintenance of health-related quality of life and performance status in the BVZ group compared with the placebo group; however, overall survival (OS) did not differ significantly between the two groups⁵. In Japan, BVZ was approved in 2013 for the treatment of both newly diagnosed and recurrent high-grade glioma (HGG). Opportunities to use BVZ in combination with Stupp's regimen to treat newly diagnosed HGG are increasing, but distinctive imaging biomarkers for predicting BVZ treatment efficacy have not been elucidated.

When anti-angiogenic agents such as BVZ are used, the phenomenon of normalization of intratumoral blood vessels and decreased permeability of the blood–brain barrier have occurred within tumor tissues, which has resulted in shrinkage of contrast-enhanced lesions on MRI⁶. This phenomenon, known as a pseudo-response, occurs in 20–60% of patients treated with BVZ⁷. The Response Assessment in Neuro-Oncology (RANO) criteria, which are based on morphological changes in lesions with contrast-enhanced and T2/fluid-attenuated inversion recovery (FLAIR) hyperintensity⁸, might be suitable for response assessment in patients with HGG treated with BVZ. However, the RANO criteria have not reached complete consensus because it is difficult to discriminate

¹Division of Neurosurgery, Department of Brain and Neurosciences, Faculty of Medicine, Tottori University, 36-1, Nishi-cho, Yonago 683-8504, Tottori, Japan. ²Division of Pathology, Department of Pathology, Faculty of Medicine, Tottori University, Yonago 683- 8504, Tottori, Japan. ✉email: kanimo@tottori-u.ac.jp

between tumor infiltration and nonneoplastic signal changes such as peritumoral edema on T2/FLAIR images^{8,9}. Thus, the establishment of reliable imaging biomarkers that predict the treatment efficacy of BVZ is desired.

In this study, we focused on calcification and diffusion restriction, which sometimes appear around the resection cavity or periventricular white matter in patients with HGG treated with BVZ, as candidate imaging biomarkers for BVZ treatment efficacy. We also investigated the mechanism underlying these unique radiological findings from a histopathological perspective.

Methods

Patients

This retrospective study included patients with newly diagnosed or recurrent HGG who received BVZ chemotherapy. Patients with newly diagnosed HGG underwent surgery followed by local radiotherapy of 40–60 Gy and chemotherapy with concomitant temozolomide (TMZ) according to Stupp's regimen¹⁰. BVZ was used in combination with Stupp's regimen in patients who underwent partial removal or had accompanying prominent peritumoral edematous changes. Patients with recurrent HGG received BVZ monotherapy or combination therapy consisting of BVZ and TMZ.

Our study was performed in accordance with the Declaration of Helsinki. The requirement of informed consent was waived by the ethics committee of Tottori University, Faculty of Medicine (No. 23A018). Of the patients with newly diagnosed or recurrent HGG who received BVZ-based chemotherapy at Tottori University Hospital (36–1, Nishi-cho, Yonago, Tottori, Japan) between June 2013 and May 2021, patients who received more than 12 cycles (6 months) of intravenous BVZ (10 mg/kg, every 2 weeks) and CT scans 6 months or more after the initial BVZ therapy were included in this study. Drug withdrawal for up to 4 weeks and dose reduction to 7 mg/kg were allowed when there were adverse events like hypertension or proteinuria. Clinical characteristics were abstracted from each patient's records.

Radiological and histopathological evaluation

A 3-Tesla MRI system (Discovery MR750w; GE Healthcare, Milwaukee, WI, USA) was used 1 month after initial BVZ therapy and every 2–3 months thereafter. For calculating PFS, disease progression was defined according to the RANO criteria. SYNAPSE VINCENT software (Fujifilm Medical System, Tokyo, Japan) was used for calculating apparent diffusion coefficient (ADC) values obtained with diffusion-weighted imaging (DWI) with a b value of 1,000 s/mm². For measuring ADC values, DWI for each patient was automatically co-registered to the ADC map. A circular 5 mm² region of interest was manually set within diffusion-restricted lesions on the ADC map (Fig. 1). Perfusion patterns within diffusion-restricted lesions were also evaluated using arterial spin labeling (ASL) imaging. ASL imaging was performed with pseudo-continuous labeling, high-level background suppression, and a stack of spirals of 3D fast spin echo for 3D volume acquisition of the entire brain. We evaluated perfusion patterns of target regions with diffusion restriction compared with corresponding areas on the contralateral side of the brain but we did not quantify perfusion. DWI for each patient was automatically co-registered to the ASL color cerebral blood flow map using SYNAPSE VINCENT. According to a previous study¹¹, hyperperfusion was defined as a higher color scale in the target region than in the corresponding region on the contralateral side. Similarly, hypoperfusion was defined as a lower color scale in the target region. CT

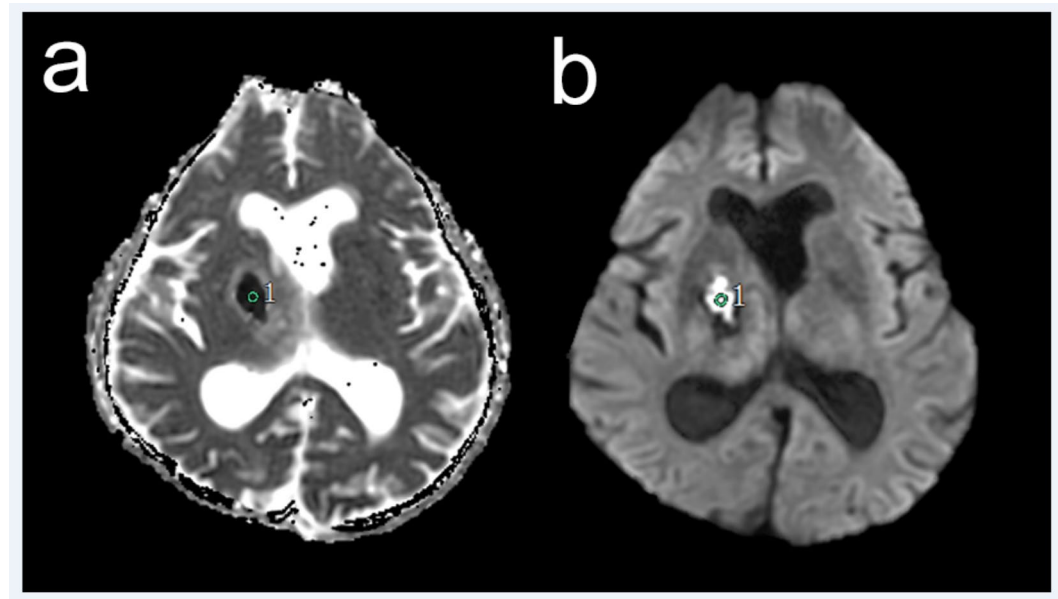


Fig. 1. A circular 5 mm² region of interest was set on an apparent diffusion coefficient (ADC) map (a) and diffusion-weighted imaging (b) centered around the diffusion-restricted area for calculating ADC values using SYNAPSE VINCENT software.

scans were performed when patients were transported to our hospital by ambulance due to a seizure or when calcification was suspected on susceptibility-weighted MRI. One patient with newly diagnosed glioblastoma had a contraindication to MRI (cardiac pacemaker). For this patient, we performed CT for follow-up imaging every 2 months after the initiation of BVZ treatment. To confirm spatial coincidence of calcification and diffusion-restricted lesions, DWI of each patient in the calcification group was automatically co-registered to CT imaging using SYNAPSE VINCENT. All radiological evaluations were carried out by two investigators (T.H. and A.K.) in a blinded fashion. If their evaluations were not concordant, the two investigators reached a consensus opinion.

Immunohistochemical studies on formalin-fixed paraffin-embedded tissues were performed using antibodies specific for isocitrate dehydrogenase 1 (IDH-1) R132H mutation and O6-methylguanine DNA methyltransferase (MGMT) to evaluate for IDH-1 mutations and MGMT protein expression in all patients. Histopathological evaluation of BVZ-induced calcifications was performed with hematoxylin–eosin (H–E) and immunohistochemical staining for CD34 and hypoxia-inducible factor 1 α (HIF-1 α). Two samples selectively resected during repeat surgery to treat recurrence after BVZ treatment were evaluated. Tumor Sect. (4 μ m) were subjected to immunohistochemistry for CD34, HIF-1 α , IDH-1 R132H, and MGMT. Deparaffinized and rehydrated slides were autoclaved for 10 min in citrate buffer (pH 6.0). Endogenous peroxidase was blocked by incubating the slides in 3% H_2O_2 for 10 min. The slides were incubated overnight at 4 °C with rabbit monoclonal anti-CD34 antibody (1:2500, ab81289; Abcam, Waltham, MA, USA) and rabbit polyclonal anti-HIF-1 α antibody (1:100, GTX127309, GeneTex, San Antonio, TX, USA). Tissue labeling for these antigens was performed using the Vectastain Elite ABC Universal Plus kit (Vector Laboratories, Burlingame, CA, USA) with standardized protocols.

Statistical analysis

JMP (SAS, Cary, NC, USA) version 16.2 was used for all statistical analyses. Statistical significance was set at $P < 0.05$. Baseline patient characteristics were compared using a two-sided Fischer's exact test for categorical variables. The number of BVZ cycles was dichotomized based on the median value. The Mann–Whitney U test was used to compare ADC values of diffusion-restricted lesions that appeared after BVZ therapy between the calcification and non-calcification groups. To analyze whether calcification on CT can be used to predict long-term prognosis, survival was analyzed based on the Kaplan–Meier curve and log-rank test. OS was defined as the duration from the date of initial BVZ treatment to the date of death or last follow-up. PFS was defined as the duration from the date of initial BVZ treatment to the date of disease progression or last follow-up. Patients who remained alive at the end of the observation period or who were lost to follow-up within the observation period were censored.

Results

Table 1 shows the baseline patient characteristics. Thirty-five patients, 21 males (60.0%) and 14 females (40.0%), were eligible for this study. The median age at initial BVZ treatment was 61 years (interquartile range [IQR], 42–70). Calcification around the resection cavity or periventricular white matter was identified using CT in 17

| Variable | | Calcification | Non-calcification | <i>p</i> value ^a |
|-------------------------|---------------|---------------|-------------------|-----------------------------|
| All patients | | 17 (48.6%) | 18 (51.4%) | |
| Age (years) | ≥ 65 | 8 (47.1%) | 7 (38.9%) | 0.738 |
| | < 65 | 9 (52.9%) | 11 (61.1%) | |
| Sex | Male | 9 (52.9%) | 12 (66.7%) | 0.500 |
| | Female | 8 (47.1%) | 6 (33.3%) | |
| BVZ treatment | New diagnosis | 10 (58.8%) | 10 (55.6%) | > 0.999 |
| | Recurrence | 7 (41.2%) | 8 (44.4%) | |
| WHO grade | 3 | 8 (47.1%) | 9 (50.0%) | > 0.999 |
| | 4 | 9 (52.9%) | 9 (50.0%) | |
| IDH-1 mutation | Yes | 4 (26.7%) | 4 (23.5%) | > 0.999 |
| | No | 11 (73.3%) | 13 (76.5%) | |
| MGMT protein expression | Present | 10 (66.7%) | 10 (58.8%) | 0.708 |
| | Absent | 5 (33.3%) | 7 (41.2%) | |
| Number of BVZ cycles | ≥ 23 | 13 (76.5%) | 6 (33.3%) | 0.018 |
| | < 23 | 4 (23.5%) | 12 (66.7%) | |
| BCNU wafer implantation | Yes | 8 (47.1%) | 9 (50.0%) | > 0.999 |
| | No | 9 (52.9%) | 9 (50.0%) | |
| Extent of resection | ≥ 90% | 6 (35.3%) | 10 (55.6%) | 0.315 |
| | < 90% | 11 (64.7%) | 8 (44.4%) | |

Table 1. Baseline patient characteristics. ^aTwo-sided Fisher's exact test. Abbreviations: BCNU, bis-chloroethyl nitrosourea; BVZ, bevacizumab; IDH-1, isocitrate dehydrogenase 1; MGMT, O6-methylguanine DNA methyltransferase; WHO, World Health Organization.

(48.6%) of 35 patients at a median of 12 months after starting BVZ treatment, 12 months in patients with newly diagnosed HGG, and 9 months in patients with recurrent HGG.

We compared baseline patient characteristics between the calcification group ($n=17$) and the non-calcification group ($n=18$) (Table 1). There were no significant differences between the two groups in terms of age, sex, timing of BVZ initiation, World Health Organization (WHO) morphological grade, IDH-1 mutation status, MGMT protein expression, bis-chloroethyl nitrosourea (BCNU) wafer implantation, or extent of resection. The median number of BVZ cycles was 38 (IQR, 22–53) in the calcification group and 20 (IQR, 10–24) in the non-calcification group, respectively ($p=0.0176$).

Calcification and survival

In this study, we defined PFS and OS based on the initiation of BVZ treatment. Figure 2 shows the OS and PFS of the calcification and non-calcification groups based on the Kaplan–Meier method. The median PFS and OS of the non-calcification group were 7 (IQR, 5–16) and 12 (IQR, 10–18) months, respectively. Those of the calcification group were 16 (IQR, 12–30) and 36 (IQR, 20–90) months, respectively. Patients in the calcification group had significantly longer PFS (Hazard Ratio [HR], 0.33; 95% Confidence Interval [CI], 0.15–0.71; $p=0.0023$) and OS (HR, 0.27; 95% CI, 0.12–0.60; $p=0.0006$) than the non-calcification group (Fig. 2a and b). When the analysis was restricted to patients with newly diagnosed HGG, the calcification group had longer PFS (HR, 0.21; 95% CI, 0.05–0.66; $p=0.0064$) and OS (HR, 0.22; 95% CI, 0.06–0.68; $p=0.0011$) (Fig. 2c and d).

Diffusion-restricted lesions and ADC values

In 12 (70.6%) of 17 patients with calcification (Table 2), diffusion-restricted lesions coincided spatially with calcifications observed around the resection cavity or periventricular white matter (Fig. 3). These areas were always observed prior to the appearance of calcification, at a median of approximately 4.5 months after the initiation of BVZ treatment (Table 2). In all 12 patients, the size of diffusion-restricted lesions remained stable during a median duration of 5.5 (IQR, 2.3–19.0) months. On ASL imaging, diffusion-restricted lesions in all patients had hypoperfusion (Fig. 4a). Conversely, once diffusion-restricted lesions appeared in the non-calcification group, they gradually increased in size on DWI and had hyperperfusion on ASL imaging in all

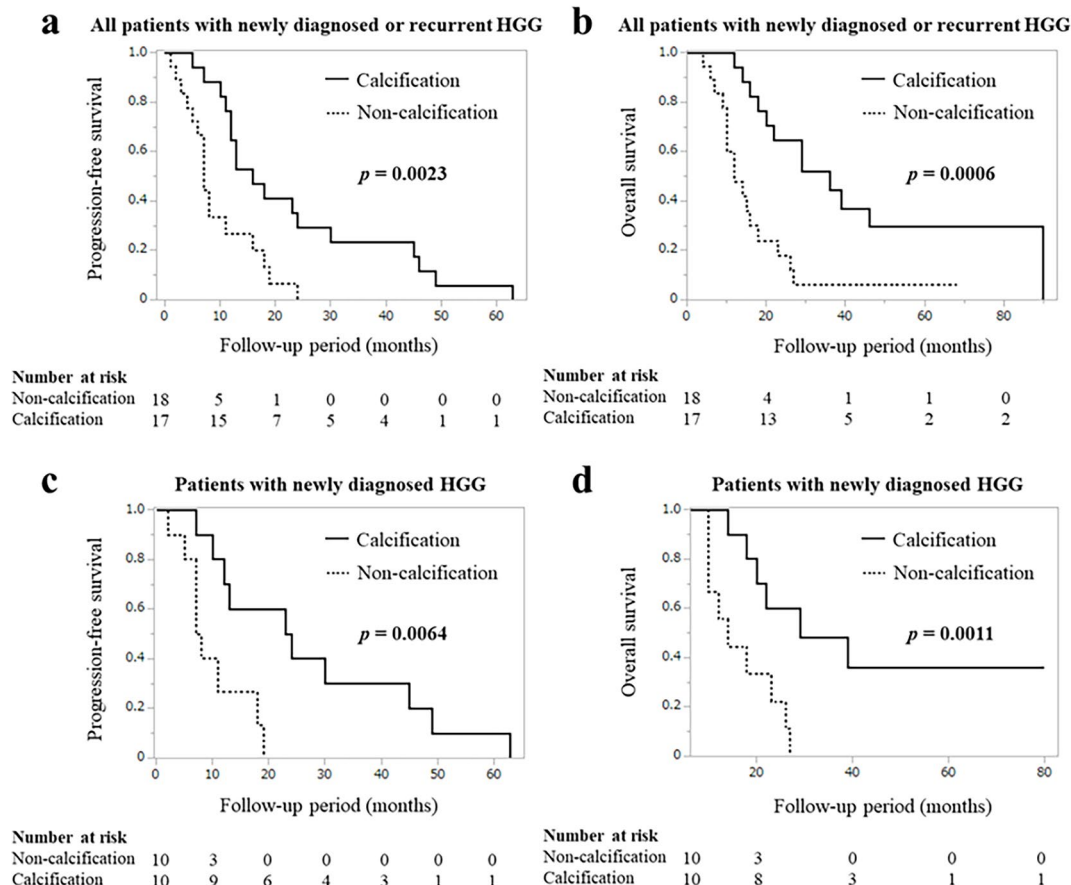


Fig. 2. Kaplan–Meier survival curves for progression-free survival and overall survival in the calcification group (solid lines) and the non-calcification group (dashed lines). **a, b:** Analysis of all patients with newly diagnosed or recurrent high-grade glioma (HGG). **c, d:** Analysis restricted to patients with newly diagnosed HGG. p values were calculated with the log-rank test.

| Patient | Sex | Age (years) | WHO grade | BCNU wafer | Timing of BVZ | Number of BVZ cycles | Timing of onset (months) | |
|---------|-----|-------------|-----------|------------|---------------|----------------------|--------------------------|---------------|
| | | | | | | | Diffusion restriction | Calcification |
| 1 | M | 42 | 3 | No | R | 40 | 4 | 6 |
| 2 | M | 39 | 3 | No | N | 76 | 2 | 32 |
| 3 | F | 73 | 3 | No | N | 38 | 1 | 26 |
| 4 | M | 66 | 3 | No | N | 20 | 5 | 10 |
| 5 | M | 40 | 4 | Yes | N | 74 | 10 | 16 |
| 6 | F | 22 | 3 | No | N | 51 | 3 | 6 |
| 7 | M | 65 | 4 | Yes | N | 55 | 2 | 50 |
| 8 | M | 35 | 3 | No | R | 66 | 20 | 20 |
| 9 | M | 61 | 4 | Yes | N | 25 | 11 | 12 |
| 10 | M | 70 | 4 | Yes | N | 10 | 9 | 10 |
| 11 | F | 54 | 4 | Yes | R | 29 | 6 | 8 |
| 12 | M | 66 | 4 | Yes | N | 23 | 1 | 12 |
| Median | | 58 | | | | 39 | 4.5 | 12 |

Table 2. Summary of 12 cases of calcification with diffusion restriction areas. Abbreviations: BCNU, bis-chloroethyl nitrosourea; BVZ, bevacizumab; F, female; M, male; N, new diagnosis; R, recurrence; WHO, World Health Organization.

patients. These areas were ultimately diagnosed as recurrent lesions (Fig. 4b). We compared the ADC values of the two groups when diffusion-restricted lesions first appeared. The diffusion-restricted lesions in the calcification group had significantly lower ADC values than those in the non-calcification group (median, 0.56×10^{-3} mm 2 /s; IQR, 0.46–0.59 vs. median, 0.90×10^{-3} mm 2 /s; IQR, 0.84–0.99; $p = 0.0031$) based on the Mann–Whitney U test (Fig. 5).

Histopathological findings

We were able to evaluate regions with calcifications within resected tissues in two patients with recurrent tumor using a histopathological approach (Fig. 6). One patient was a 39-year-old male with IDH-1 mutant astrocytoma, WHO grade 3 (Patient 2 in Table 2). The other patient was a 54-year-old female with IDH wild-type glioblastoma, WHO grade 4 (Patient 11 in Table 2). In both patients with calcification, microcalcifications were scattered within necrotic tissue and a few viable glioma cells were observed around these tissues on H–E staining. We speculated that necrosis was the result of hypoxia due to BVZ-induced anti-angiogenetic activity. Thus, we examined the expression of CD34 and HIF-1 α to evaluate microvessel density (MVD) and hypoxia status of specimens with immunohistochemical staining. There was less expression of CD34 in the core lesion of recurrent tumor tissue than in the initial tumor tissue, but the expression was further decreased in calcification lesions. By contrast, the expression of HIF-1 α was positive in both calcification lesions and the recurrent tumor core lesion, but not in the initial tumor lesion.

Discussion

BVZ is widely used to treat recurrent HGG. However, imaging or pathological biomarkers for predicting BVZ efficacy have not been elucidated¹². In this study, we first analyzed the relationship between the appearance of calcification and BVZ treatment and explored calcification as a candidate imaging biomarker for BVZ efficacy. In approximately half of the patients who received BVZ for newly diagnosed or recurrent HGG, calcification was identified around the resection cavity or periventricular white matter at a median of 12 months after initiating BVZ treatment. When we defined PFS and OS based on the initiation of BVZ treatment, patients in the calcification group had a favorable prognosis, with PFS that was twice as long and OS that was three times as long as patients in the non-calcification group (Fig. 2). Blumenthal et al¹³ reported that median OS for patients with HGG and calcification who received BVZ is significantly longer than median OS in those without calcification (25.2 months vs. 11.1 months; $p = 0.03$). These findings suggest that the appearance of calcification in patients with HGG treated with BVZ can be a significant predictor for BVZ efficacy.

In most patients with calcification, diffusion-restricted lesions coincided with calcification on CT (Fig. 3). These lesions were always observed prior to the appearance of calcification. Furthermore, diffusion-restricted lesions in the calcification group had significantly lower ADC values than those in the non-calcification group (Fig. 5). Since diffusion-restricted lesions appeared approximately a median of 4.5 (IQR, 1–20) months earlier than calcifications (12.0 months) after the initiation of BVZ treatment (Table 2), they seem to be useful as a favorable prognostic factor in patients with HGG treated with BVZ to judge treatment response to BVZ at an earlier stage. Bähr et al. reported the appearance of T1 hyperintense lesions at a median of 55 days and subsequently identified calcification at a median of 163 days after the initiation of BVZ treatment in some patients with recurrent glioblastoma¹⁴. They argue that T1 hyperintense lesions are related to the presence of calcification because the calcified areas shortened the T1 relaxation time of protons next to the surface of the calcium crystals¹⁵. In the present study, 7 (41.2%) of 17 patients in the calcification group had T1 hyperintense lesions prior to the appearance of calcifications at a median of 9.0 months after BVZ initiation, which was lower than the proportion of patients with the appearance of diffusion-restricted lesions (12 of 17 patients, 70.6%). T1

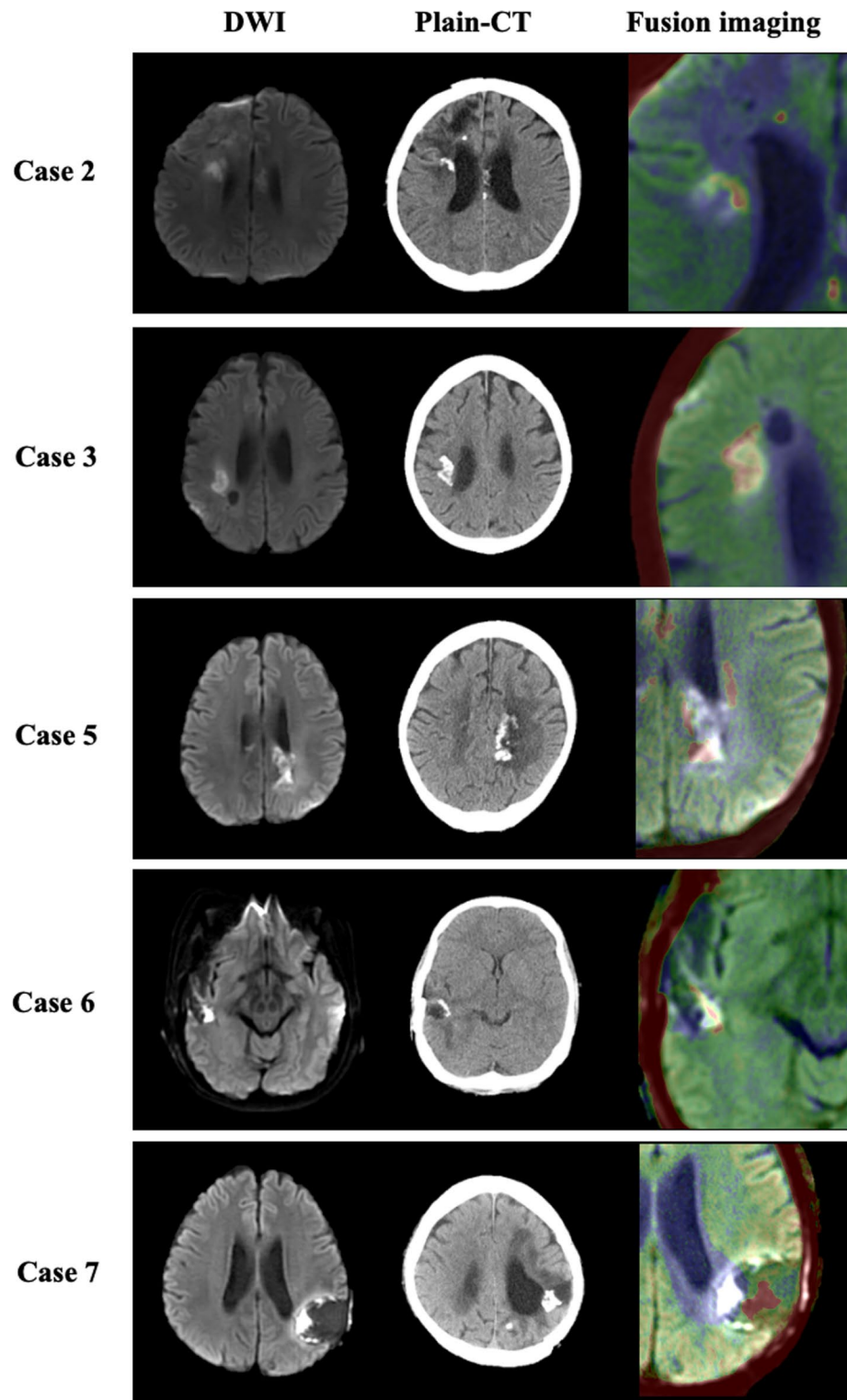


Fig. 3. Diffusion-restricted areas on diffusion-weighted imaging (DWI) (first column) and calcification lesions on plain CT (second column) were merged to create fusion images (third column) using SYNAPSE VINCENT software in five cases with calcification (Cases 2, 3, 5–7 in Table 2). Calcifications appear as red areas and diffusion-restricted lesions appear as white areas on the merged images.

hyperintense lesions appeared in the same areas as diffusion-restricted lesions at the same time (three patients) or later (two patients). However, the remaining two patients did not develop diffusion-restricted lesions. Hence, the sensitivity and specificity of T1 hyperintense lesions seem somewhat lower than those of diffusion-restricted lesions.

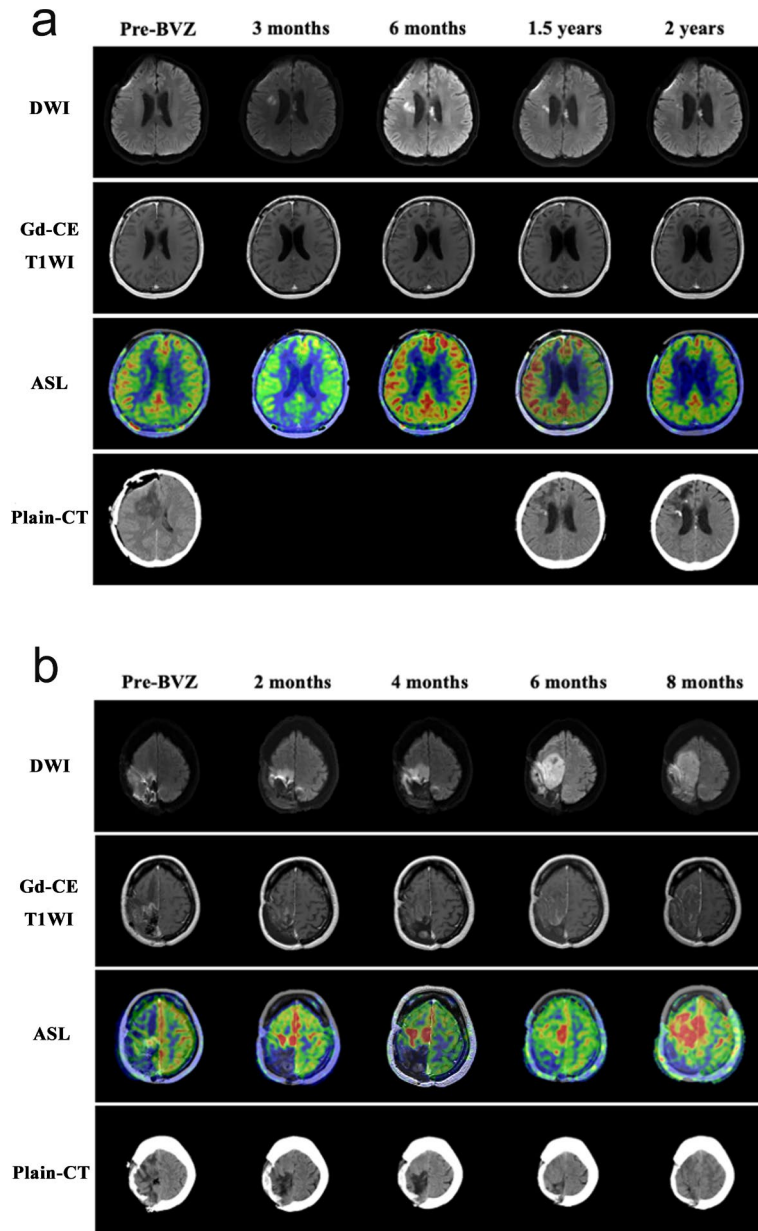


Fig. 4. Representative patients included a 39-year-old male with World Health Organization (WHO) grade 3 astrocytoma, in the calcification group (a, Patient 2 in Table 2) and a 39-year-old female with WHO grade 4 glioblastoma in the non-calcification group (b). Diffusion-weighted imaging; DWI (first row), gadolinium contrast-enhanced (Gd-CE) T1 weighted imaging (T1WI) (second row), arterial spin labeling (ASL) imaging (third row), and plain CT (fourth row) during the clinical course before and after bevacizumab (BVZ) therapy are shown. In the calcification group, diffusion-restricted lesions remained stable in size and had hypoperfusion on ASL imaging (a). Conversely, once diffusion-restricted lesions appeared in the non-calcification group, they gradually increased in size and had hyperperfusion on ASL imaging (b).

Histopathological examination of calcified regions showed scattered microcalcifications inside necrotic tissue surrounded by a few viable glioma cells on H-E staining (Fig. 6). Immunohistochemical staining indicated decreased MVD on CD34 staining and tissue hypoxia based on HIF-1 α staining in calcifications. Considering these histopathological findings, the development of necrosis was related to the decrease in MVD followed by chronic tissue hypoxia. BVZ is known to decrease MVD and increase intratumoral hypoxia¹⁶, leading to a decrease in CD34 expression and an increase in HIF-1 α expression in tumor tissues after BVZ treatment¹⁷. It is easy to induce tissue degeneration and ischemic changes in the area around the resection cavity with BCNU wafer placement and postoperative focal radiotherapy, which result in necrosis appearing as diffusion-restricted areas on DWI. We also confirmed the appearance of diffusion-restricted lesions around the periventricular white matter in patients with tumors involving the periventricular area. This phenomenon might be associated with anatomical factors related to cerebral blood supply because the periventricular zone is initially intolerant

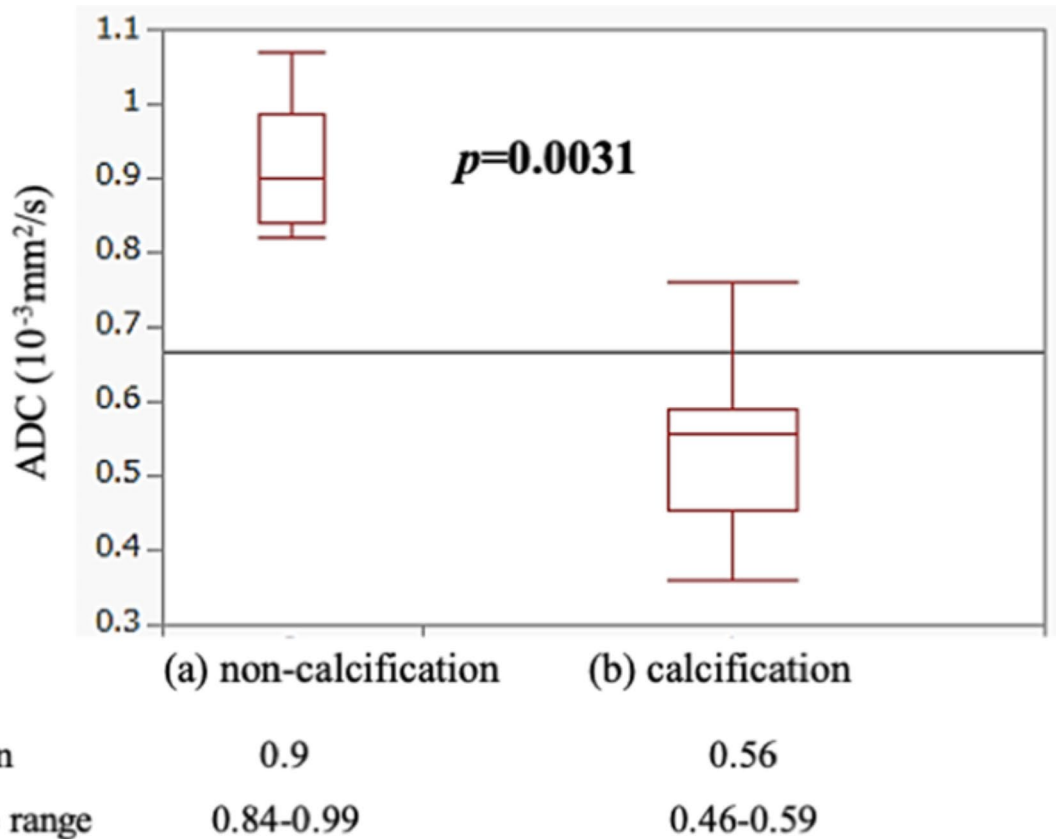


Fig. 5. Apparent diffusion coefficient (ADC) values of diffusion-restricted lesions in the non-calcification (a) and calcification groups (b) were compared.

to ischemic damage¹⁸. Furthermore, considering the mechanism leading to BVZ-induced calcifications based on histopathological findings, we hypothesize that these calcifications are related to dystrophic calcification; endogenous calcium is released and deposited in degenerated or necrotic tissues by injurious agents like BVZ¹⁹.

Oligodendroglial tumors are known to frequently have calcifications in tumor tissue. Khalid et al. reported that tumor calcification is more common in grade 3 oligodendroglomas; calcification was identified in 25.0% of grade 2 tumors and 52.4% of grade 3 tumors²⁰. Two patients with grade 3 oligodendrogloma were included in this study. One patient was in the non-calcification group. The other patient was in the calcification group, but a new calcified lesion appeared far from the originally identified calcification 6 months after the initiation of BVZ treatment. In addition to tumor phenotype, long-term clinical course could also be relevant to calcification²¹. However, Blumenthal et al. reported that patients with HGG treated with BVZ are more likely to develop calcification than non-treated patients¹³. Table 1 shows that the calcification group had more BVZ cycles than the non-calcification group. Long-term use of BVZ is likely to induce calcification, which might be related to good responsiveness to BVZ treatment, resulting in a favorable clinical course. In patients with metastatic colorectal cancer treated with BVZ, Zhou et al. reported that calcification is associated with better survival²².

DWI is a form of MRI based on visualization of the random Brownian motion of water molecules in living tissue. In general, hypercellularity and necrosis restrict the diffusion of water molecules in the extracellular space, which results in a high signal on DWI and a low signal on ADC imaging in brain tumors, including gliomas^{23,24}. In previous reports, the presence of BVZ-induced diffusion-restricted lesions in patients with HGG has been reported²³⁻³¹, but there is no consensus about the mechanism and significance of this phenomenon. Some authors have demonstrated that BVZ-induced diffusion-restricted lesions predominantly represent necrosis, not aggressive hypercellularity, on the basis of pathological examination of biopsy specimens^{23,26,27,29}. Mong et al. reported that the appearance of persistent diffusion-restricted lesions after BVZ administration is a favorable prognostic factor²⁹. By contrast, some authors have reported that diffusion-restricted lesions reflect aggressive infiltrative tumor and result in worse OS^{30,31}. In our study, diffusion-restricted lesions in the calcification group had significantly lower ADC values than those in the non-calcification group (Fig. 5), suggesting that measuring ADC values might enable us to identify patients with truly favorable prognosis. This finding is similar to those in previous reports where ADC values of diffusion-restricted lesions that were pathologically demonstrated as areas with necrosis were significantly lower than those of hypercellular lesions in patients with glioma treated with BVZ^{23,24}. Nguyen et al. reported that the optimal ADC threshold for differentiating between hypercellularity and necrosis is $0.736 \times 10^{-3} \text{ mm}^2/\text{s}$.²³ These areas usually have low cerebral blood flow and cerebral blood volume on MR perfusion imaging, suggesting the utility of differentiating between necrosis and recurrent lesions^{26,27,29}.

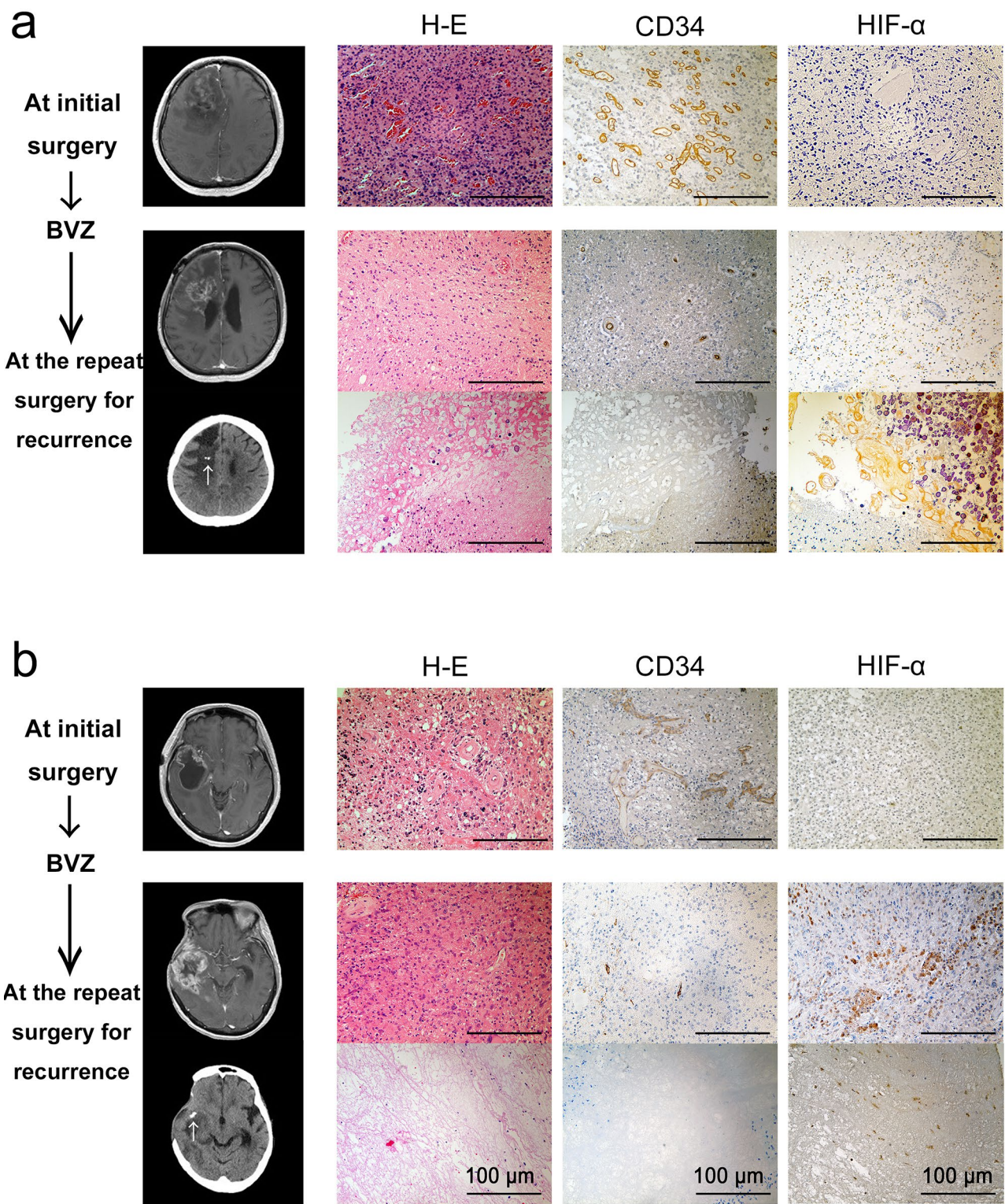


Fig. 6. Histopathological features in the calcification group are shown. Patient 2 (a) had World Health Organization (WHO) grade 3 astrocytoma and was positive for isocitrate dehydrogenase 1 (IDH-1) R132H and O6-methylguanine DNA methyltransferase (MGMT) protein. Patient 11 (b) had WHO grade 4 glioblastoma and was negative for IDH-1 R132H and MGMT protein. Gadolinium contrast-enhanced (Gd-CE) T1 weighted imaging (T1WI) at the time of initial onset (upper), Gd-CE T1WI (middle row) and plain CT showing calcification (white arrows on CT, lower row) at the time of recurrence under bevacizumab (BVZ) treatment are also shown. The initial tumor tissue (upper row), core lesion (middle row), and calcification (lower row) of recurrent tumor tissue were compared with hematoxylin–eosin (H-E) staining and immunohistochemistry for CD34 and hypoxia-inducible factor 1 α (HIF-1 α). All scale bars, 100 μ m.

Indeed, in the present study, all persistent diffusion-restricted lesions in the calcification group were associated with hypoperfusion on ASL (Fig. 4a). However, as shown in Fig. 4b, progressive diffusion-restricted lesions in the non-calcification group were associated with hyperperfusion, suggesting an increase in cell density due to tumor recurrence. In addition to the measurement of ADC values, hypoperfusion on MR perfusion imaging supports the hypothesis that diffusion-restricted lesions correspond to treatment-related necrosis, not tumor recurrence, in patients with HGG treated with BVZ. The radiological and histopathological findings in this study suggest that long-term BVZ treatment leads to the development of calcification within necrotic tissue via dystrophic calcification, which is consistent with the hypothesis that the development of persistent diffusion restriction is followed by calcification. If diffusion-restricted lesions appear around the resection cavity or periventricular zones after the initiation of BVZ treatment, it is necessary to check ADC values and perform MR perfusion imaging. Under these circumstances, we need to keep in mind that it is important to patiently continue BVZ treatment, considering the possibility of a favorable prognosis rather than interrupting treatment based on a misunderstanding of tumor recurrence.

Although previous clinical trials could not demonstrate a survival benefit with BVZ, we speculate that some patients were withdrawn from BVZ treatment because diffusion-restricted lesions were considered to indicate tumor recurrence or cerebral infarction. Thus, prolonged survival with BVZ might be achieved if the patients who will benefit from BVZ treatment are appropriately selected according to the imaging biomarkers suggested in this study. Another novel result of this study is that prolonged survival in the calcification group was also observed in the analysis restricted to patients with newly diagnosed HGG. Although BVZ treatment for newly diagnosed HGG has been approved only in Japan, the above result might lead to expanding indications of BVZ for newly diagnosed HGG in the future.

This study was limited by its retrospective design and the relatively small population size. Follow-up CT scans were not performed routinely; thus, we could not determine the exact date of calcification onset. However, one patient who only underwent follow-up CT imaging had calcifications around the resection cavity at 10 months after the initiation of BVZ treatment (data not shown), which was almost the same time that calcifications appeared in the calcification group of this study. Berger et al. reported that prolonged brain retraction during glioma surgery may result in rim restriction on postoperative imaging³². In this study, two newly diagnosed cases exhibited diffusion restriction areas prior to calcification one month after the initiation of BVZ treatment. Although diffusion restriction areas were not observed on postoperative MRI in these cases, the potential influence of surgical manipulation cannot be entirely dismissed. We evaluated perfusion patterns qualitatively, but a quantitative method might be more preferable. Another limitation of this study was that histopathological validation was performed only in 2 of 17 patients with calcification. It was impossible for most patients because tumor resection was not included as a routine option to treat recurrence. However, correlated imaging variation in the calcification group suggests that calcification occurs under similar circumstances and is a secondary product of efficacious BVZ treatment. Because these radiological and pathological findings might facilitate the use of BVZ, a larger sample or large-scale studies are warranted to perform a more detailed characterization and stratification of patients treated with BVZ.

Conclusions

This is the first report that could evaluate persistent diffusion restriction followed by calcification in patients with HGG treated with BVZ from a histopathological perspective. Calcifications usually appear around the resection cavity or periventricular zone, where it is initially easy to induce tissue degeneration and ischemic damage. We speculate that this phenomenon is a secondary product of long-term BVZ use due to its good responsiveness and the appearance of calcifications can be an imaging biomarker for predicting a favorable clinical course. In BVZ-induced diffusion-restricted lesions, low ADC values and hypoperfusion indicate necrosis rather than tumor recurrence. It is important to patiently continue BVZ treatment in such patients.

Data availability

The data that support the findings of this study are available on request from the corresponding author. The data are not publicly available due to ethical restrictions.

Received: 13 May 2024; Accepted: 29 October 2024

Published online: 02 November 2024

References

1. Melincovici, C. S. et al. Vascular endothelial growth factor (VEGF) - key factor in normal and pathological angiogenesis. *Rom J Morphol Embryol.* **59**, 455–467 (2018).
2. Al-Abd, A. M., Alamoudi, A. J., Abdel-Naim, A. B., Neamatallah, T. A. & Ashour, O. M. Anti-angiogenic agents for the treatment of solid tumors: potential pathways, therapy and current strategies - a review. *J. Adv. Res.* **8**, 591–605. <https://doi.org/10.1016/j.jare.2017.06.006> (2017).
3. Vredenburgh, J. J. et al. Bevacizumab plus Irinotecan in recurrent glioblastoma multiforme. *J. Clin. Oncol.* **25**, 4722–4729. <https://doi.org/10.1200/jco.2007.12.2440> (2007).
4. Kreisl, T. N. et al. Phase II trial of single-agent bevacizumab followed by bevacizumab plus irinotecan at tumor progression in recurrent glioblastoma. *J. Clin. Oncol.* **27**, 740–745. <https://doi.org/10.1200/jco.2008.16.3055> (2009).
5. Chinot, O. L. et al. Bevacizumab plus radiotherapy-temozolamide for newly diagnosed glioblastoma. *N Engl. J. Med.* **370**, 709–722. <https://doi.org/10.1056/NEJMoa1308345> (2014).
6. Ellingson, B. M. et al. Quantitative volumetric analysis of conventional MRI response in recurrent glioblastoma treated with bevacizumab. *Neuro Oncol.* **13**, 401–409. <https://doi.org/10.1093/neuonc/noq206> (2011).
7. Arevalo, O. D. et al. Assessment of Glioblastoma Response in the era of Bevacizumab: Longstanding and Emergent challenges in the imaging evaluation of Pseudoresponse. *Front. Neurol.* **10**, 460. <https://doi.org/10.3389/fneur.2019.00460> (2019).

8. Wen, P. Y. et al. Updated response assessment criteria for high-grade gliomas: response assessment in neuro-oncology working group. *J. Clin. Oncol.* **28**, 1963–1972. <https://doi.org/10.1200/jco.2009.26.3541> (2010).
9. Hutterer, M., Hattingen, E., Palm, C., Proescholdt, M. A. & Hau, P. Current standards and new concepts in MRI and PET response assessment of antiangiogenic therapies in high-grade glioma patients. *Neuro Oncol.* **17**, 784–800. <https://doi.org/10.1093/neuonc/nou322> (2015).
10. Stupp, R. et al. Radiotherapy plus concomitant and adjuvant temozolomide for glioblastoma. *N Engl. J. Med.* **352**, 987–996. <https://doi.org/10.1056/NEJMoa043330> (2005).
11. Chen, T. Y. et al. Arterial spin-labeling in routine clinical practice: a preliminary experience of 200 cases and correlation with MRI and clinical findings. *Clin. Imaging.* **36**, 345–352. <https://doi.org/10.1016/j.clinimag.2011.11.003> (2012).
12. Manneh Kopp, R. A. et al. Correlation of radiological and immunochemical parameters with clinical outcome in patients with recurrent glioblastoma treated with Bevacizumab. *Clin. Transl Oncol.* **21**, 1413–1423. <https://doi.org/10.1007/s12094-019-02070-6> (2019).
13. Blumenthal, D. T. et al. Calcification in high grade gliomas treated with bevacizumab. *J. Neurooncol.* **123**, 283–288. <https://doi.org/10.1007/s11060-015-1796-z> (2015).
14. Bähr, O., Hattingen, E., Rieger, J. & Steinbach, J. P. Bevacizumab-induced tumor calcifications as a surrogate marker of outcome in patients with glioblastoma. *Neuro Oncol.* **13**, 1020–1029. <https://doi.org/10.1093/neuonc/nor099> (2011).
15. Henkelman, R. M., Watts, J. F. & Kucharczyk, W. High signal intensity in MR images of calcified brain tissue. *Radiology.* **179**, 199–206. <https://doi.org/10.1148/radiology.179.1.1848714> (1991).
16. Rapisarda, A. et al. Increased antitumor activity of bevacizumab in combination with hypoxia inducible factor-1 inhibition. *Mol. Cancer Ther.* **8**, 1867–1877. <https://doi.org/10.1158/1535-7163.Mct-09-0274> (2009).
17. Fan, Y. et al. Metformin anticancer: reverses tumor hypoxia induced by bevacizumab and reduces the expression of cancer stem cell markers CD44/CD117 in human ovarian cancer SKOV3 cells. *Front. Pharmacol.* **13** <https://doi.org/10.3389/fphar.2022.955984> (2022).
18. De Reuck, J. & vander Eecken, H. The anatomy of the late radiation encephalopathy. *Eur. Neurol.* **13**, 481–494. <https://doi.org/10.1159/000114704> (1975).
19. Chan, E. D., Morales, D. V., Welsh, C. H., McDermott, M. T. & Schwarz, M. I. Calcium deposition with or without bone formation in the lung. *Am. J. Respir Crit. Care Med.* **165**, 1654–1669. <https://doi.org/10.1164/rccm.2108054> (2002).
20. Khalid, L. et al. Imaging characteristics of Oligodendrogiomas that Predict Grade. *Am. J. Neuroradiol.* **33**, 852–857. <https://doi.org/10.3174/ajnr.A2895> (2012).
21. Lote, K., Egeland, T., Hager, B., Skullerud, K. & Hirschberg, H. Prognostic significance of CT contrast enhancement within histological subgroups of intracranial glioma. *J. Neurooncol.* **40**, 161–170. <https://doi.org/10.1023/a:1006106708606> (1998).
22. Zhou, Y. W., Long, Y. X., Liu, X., Liu, J. Y. & Qiu, M. Tumor calcification is associated with better survival in metastatic colorectal cancer patients treated with bevacizumab plus chemotherapy. *Future Oncol.* **18**, 2453–2464. <https://doi.org/10.2217/fon-2021-1422> (2022).
23. Nguyen, H. S. et al. Progressing Bevacizumab-Induced Diffusion Restriction is Associated with Coagulative Necrosis surrounded by viable tumor and decreased overall survival in patients with recurrent glioblastoma. *AJNR Am. J. Neuroradiol.* **37**, 2201–2208. <https://doi.org/10.3174/ajnr.A4898> (2016).
24. Zakhari, N. et al. Diagnostic accuracy of centrally restricted diffusion in the differentiation of treatment-related necrosis from Tumor Recurrence in High-Grade Gliomas. *AJNR Am. J. Neuroradiol.* **39**, 260–264. <https://doi.org/10.3174/ajnr.A5485> (2018).
25. Agarwal, A., Desai, A., Gupta, V. & Vibhute, P. Bevacizumab-induced coagulative necrosis with restricted diffusion. *Radiol. Imaging Cancer.* **4**, e220089. <https://doi.org/10.1148/rycan.220089> (2022).
26. Rieger, J. et al. Bevacizumab-induced diffusion-restricted lesions in malignant glioma patients. *J. Neurooncol.* **99**, 49–56. <https://doi.org/10.1007/s11060-009-0098-8> (2010).
27. Farid, N. et al. Restriction-Spectrum Imaging of Bevacizumab-Related Necrosis in a patient with GBM. *Front. Oncol.* **3**, 258. <https://doi.org/10.3389/fonc.2013.00258> (2013).
28. Futterer, S. F. et al. Diffusion abnormalities of the corpus callosum in patients receiving bevacizumab for malignant brain tumors: suspected treatment toxicity. *J. Neurooncol.* **118**, 147–153. <https://doi.org/10.1007/s11060-014-1409-2> (2014).
29. Mong, S. et al. Persistent diffusion-restricted lesions in bevacizumab-treated malignant gliomas are associated with improved survival compared with matched controls. *AJNR Am. J. Neuroradiol.* **33**, 1763–1770. <https://doi.org/10.3174/ajnr.A3053> (2012).
30. Cachia, D. et al. Radiographic patterns of progression with associated outcomes after bevacizumab therapy in glioblastoma patients. *J. Neurooncol.* **135**, 75–81. <https://doi.org/10.1007/s11060-017-2550-5> (2017).
31. Gupta, A. et al. Isolated diffusion restriction precedes the development of enhancing tumor in a subset of patients with glioblastoma. *AJNR Am. J. Neuroradiol.* **32**, 1301–1306. <https://doi.org/10.3174/ajnr.A2479> (2011).
32. Berger, A. et al. Clinical and prognostic implications of rim restriction following glioma surgery. *Sci. Rep.* **12**, 12874. <https://doi.org/10.1038/s41598-022-16717-y> (2022).

Acknowledgements

Not applicable.

Author contributions

All authors contributed to the study conception and design. Material preparation, data collection, and data analysis were performed by TH and AK. The first draft of the manuscript was written by TH and AK. All authors commented on the manuscript. All authors have read and approved the final version of the manuscript.

Funding

This study was supported by JSPS KAKENHI grant number JP23K08520 (A.K.).

Declarations

Ethics approval and consent to participate

This retrospective study was approved by the ethics committee of Tottori University, Faculty of Medicine, and the requirement for informed consent was waived because of the retrospective nature of this study (approval no. 23A018).

Competing interests

The authors declare no competing interests.

Patient consent for publication

Not applicable.

Additional information

Correspondence and requests for materials should be addressed to A.K.

Reprints and permissions information is available at www.nature.com/reprints.

Publisher's note Springer Nature remains neutral with regard to jurisdictional claims in published maps and institutional affiliations.

Open Access This article is licensed under a Creative Commons Attribution-NonCommercial-NoDerivatives 4.0 International License, which permits any non-commercial use, sharing, distribution and reproduction in any medium or format, as long as you give appropriate credit to the original author(s) and the source, provide a link to the Creative Commons licence, and indicate if you modified the licensed material. You do not have permission under this licence to share adapted material derived from this article or parts of it. The images or other third party material in this article are included in the article's Creative Commons licence, unless indicated otherwise in a credit line to the material. If material is not included in the article's Creative Commons licence and your intended use is not permitted by statutory regulation or exceeds the permitted use, you will need to obtain permission directly from the copyright holder. To view a copy of this licence, visit <http://creativecommons.org/licenses/by-nc-nd/4.0/>.

© The Author(s) 2024